Evaluation of energy and water recovery in forward osmosis–bioelectrochemical hybrid system with cellulose triacetate and polyamide asymmetric membrane in different orientations

Euntae Yang[a], Kyoung-Yeol Kim[b], Kyu-Jung Chae[c], Mi-Young Lee[a], In S. Kim[a],*

[a]School of Environmental Science and Engineering, Gwangju Institute of Science and Technology (GIST), 123 Cheomdan-gwagiro, Buk-gu, Gwangju 500-712, Korea, Tel. +82 62 715 3381; Fax: +82 62 715 2434; email: iskim@gist.ac.kr (I.S. Kim)
[b]Department of Civil and Environmental Engineering, Penn State University, University Park, PA 16802, USA
[c]Department of Environmental Engineering, Korea Maritime and Ocean University, 727 Taejong-ro, Yeongdo-Gu, Busan 606-791, Korea

ABSTRACT

Recent forward osmosis–bioelectrochemical hybrid systems (FO-BESs) have been designed to simultaneously produce bio-energy and clean water from wastewater. Asymmetric forward osmosis (FO) membranes are a crucial component for determining FO-BES performance, but only cellulose triacetate (CTA NW) membranes in the same orientation have been applied to FO-BESs. In this work, both CTA NW and polyamide (PA) membranes were tested in two membrane orientations (active layer facing feed solution or anolyte and support layer facing feed solution). For an in-depth understanding of the FO membranes, properties were investigated using scanning electron microscopy, contact angle, impedance spectroscopy, and proton transport analyses. The electricity generation and water extraction in FO-BESs having these two FO membranes in different orientations were then evaluated. Based on membrane characterization, PA seemed to be a proper membrane for the FO-BES because of higher hydrophilicity, lower membrane thickness, lower mass transfer resistance, and better proton transfer ability. However, there was no significant current output difference between the FO-BESs having CTA NW and PA. Rather, in terms of water flux, the FO-BESs having CTA NW in the support layer facing feed solution orientation showed better performance.

Keywords: Bioelectrochemial systems; Cellulose triacetate; Desalination; Forward osmosis; Membrane orientation; Polyamide

1. Introduction

Over two billion people currently dwell in water-stressed regions [1]. To alleviate water scarcity, seawater desalination and water reuse technologies have made startling progress over the past few decades. In particular, reverse osmosis membrane (RO) technologies are considered the most dependable approach among currently commercialized

*Corresponding author.

technologies, due to their low energy consumption (3–4 kWh/m^3) and high water quality [2]. However, compared to the use of conventional fresh water sources, the production cost of RO technologies is still 3.5 times higher, on average [3]. Therefore, to further reduce the cost (or energy consumption) for seawater desalination and water reuse, forward osmosis (FO) processes have been extensively explored; FO processes utilize natural osmotic pressure, created by the concentration difference between a low concentrated solution (feed solution) and a high concentrated solution (draw solution) across a double-layered semipermeable membrane, as the driving force for water production instead of applying hydraulic pressure [4].

Furthermore, FO processes have been recently developed to produce not only clean water, but also concurrently generate electricity by integrating them into bioelectrochemical systems (BESs), devices used to convert bioenergy from organic matter in wastewater into electricity using electrochemically active bacteria [5–8]. Here, this hybrid system is referred to as forward osmosis–bioelectrochemical hybrid systems (FO-BESs).

In the first study of FO-BES, the concept was investigated via a comparison to a conventional BES having a cation exchange membrane [8]. Since then, the influences of draw solutions and biofouling on membrane surfaces on bioenergy production and water flux in FO-BESs have been evaluated [6]. According to this previous study, NaCl was appropriate as the draw solution, and it was found that an acidified draw solution increased electricity generation. This study also showed that biofouling increased electricity generation but decreased water flux. In another study, FO-BESs were tested using real wastewater [7]. When real wastewater was applied, FO-BESs showed a maximum power density of 4.5 W/m^3 and a water flux of 1.3 LMH. To overcome these limitations, Werner et al. [5] applied an air-cathode to FO-BESs; according to their results, the water flux increased up to 4.1 LMH and the maximum power generation reached 43 W/m^3.

In FO-BESs, an FO membrane plays a couple of important roles. First, the FO membrane prevents mass transport between the anode and cathode chambers, except for water and protons. The FO membrane also plays a role in the filtration process for water production from wastewater. Thus, the FO membrane should be considered one of the most significant factors used to determine the performance of FO-BESs. However, most previous studies have not focused on exploring the use of different FO membranes but focused on only one type of FO membrane in the same membrane orientation. Thus, this study focuses on the effect of FO membranes on current generation and water flux in FO-BESs. Here, two different FO membranes, cellulose triacetate (CTA NW) and polyamide (PA), are characterized, and the performances of FO-BESs having these two membranes are then compared in different orientations.

2. Materials and methods

2.1. Reactor construction

Cube-shaped BES reactors having two chambers (chamber volumes: 200 mL each) were constructed. The two chambers were separated by a proton exchange membrane (PEM; working area = 5 × 5 cm; Nafion 117, Dupont Co., USA). The anodic electrodes were carbon felt (5 cm × 5 cm; 6 mm thickness; Morgan, UK) that were attached to a perforated stainless steel plate using conductive silver paste; the cathodic electrodes were perforated stainless steel (5 × 5 cm; 1.5 mm thickness; Labco Co., South Korea), coated with 0.5 mg Pt/cm^2 [9]. An Ag/AgCl reference electrode (195 mV vs. SHE; Microelectrode, USA) was installed in each chamber to measure each electrode potential. The BES reactors were inoculated with anaerobic digester sludge (20% v/v) obtained from the Gwangju Municipal Wastewater Treatment Plant in South Korea, and acclimated using artificial wastewater (pH 7), comprised of sodium acetate (200 mg/L), PBS (6,000 mg/L), nutrients, and trace mineral and vitamins, at an external resistance of 100 Ω for 2 months [10]. PBSs (50 mM, pH 7) were used for these operations. For FO-BES operations, a PEM in the BES reactors were replaced with FO membranes after the 2 months' acclimation period.

2.2. FO membrane preparation

For this study, two types of FO membranes were prepared, CTA NW (Hydration Technologies, Albany, OR) and PA (Woongjin Chemical, South Korea), and these membranes were tested in two orientations: active layer facing the feed solution (AL-FS) and support layer facing the feed solution (SL-FS). During FO-BES operation, AL-FS denotes the anode chamber facing the active layer and SL-FS denotes the anode chamber facing the support layer.

2.3. FO membrane characterization

Scanning electron microscopy (SEM; S-4700, Hitachi, Japan) was used to observe the morphology of each FO membrane. The relative hydrophobicity of

each FO membrane was determined by measuring the contact angle using a goniometer (Phoenix 300, Surface Electro Optics Co., USA).

To analyze the electrical properties of the FO membranes, a two-compartment electrodialytic cell, divided by an FO membrane (0.79 cm^2) was prepared [10]. The working volume of each compartment was 150 mL. One pair of platinum-coated titanium electrodes was inserted at the edge of each compartment to feed current into the system, and a pair of Ag/AgCl Luggin capillary reference electrodes was installed near the membrane–solution interface to monitor the potential changes across the sample membrane. The impedance spectra were measured using a potentiostat (Autolab PGSTAT 30, EcoChemie, The Netherlands) under both static and dynamic conditions, over a frequency range from 10^{-1} to 10^5 Hz. The static condition displayed no osmotic pressure difference across the FO membrane. For this condition, the two compartments of the electrodialytic cell were filled with the same concentration of NaCl solution (0.01 M). In contrast, there was an osmotic pressure difference across the FO membrane under the dynamic condition. For the dynamic condition, one chamber (feed side) contained 0.01 M NaCl solution and the other (draw side) contained 0.5 M NaCl solution.

For the proton transport test, a two-chamber abiotic cell separated by a square FO membrane (working area: 5 × 5 cm) was used. One chamber was filled with 160 mL of PBS (50 mM, pH 4) and the other was filled with 160 mL NaCl solution (600 mM, pH 7). The NaCl solution chamber was equipped with a pH meter (Orion 3-star, Thermo Scientific, USA) to monitor the pH changes by time.

2.4. FO-BES reactor operations

The FO-BESs were operated in batch mode at an external resistor of 100 Ω at room temperature (25℃) for 24 h. At the end of each fed-batch cycle, the anolyte (feed solution) and catholyte (draw solution) were replaced with new solutions after rinsing each chamber with deionized water. For these experiments, the anolyte was the artificial water used for acclimation and the catholyte was artificial seawater that was prepared by dissolving 35,000 mg of NaCl in 1 L of deionized water. Artificial wastewater (165 mL) was purged with nitrogen to remove dissolved oxygen before filling the anode chamber. To maintain a constant anolyte volume in the anode chamber during each fed-batch cycle, oxygen-free deionized water was directly supplemented to the anode chamber from a reservoir (Fig. 1). During each fed-batch cycle, 500 mL

of artificial seawater was recirculated from the catholyte and an external reservoir using a peristaltic pump (Masterflex, USA) at a flow rate of 10 mL/min. Each chamber was stirred using a magnetic bar at 300 rpm.

2.5. Experimental measurements and calculations

The weight changes of the reservoir connected to the cathode chamber for the catholyte recirculation were measured using a digital scale in order to calculate the water flux through the FO membrane. The anode and cathode potentials and overall cell voltage were measured using a multimeter (Keithley Instruments, USA) at 10-min intervals. For both the anolyte and catholyte, the pH was measured using a pH meter, and the total dissolved solids (TDS) and conductivities were determined using a TDS meter (EC-40 N, iSTEK, South Korea) at the start and end of every fed-batch cycle. The current (I) was determined using $= U/R_e$, where U is the measured voltage, and R_e is the external resistance. The coulombic efficiencies (CE) were calculated using CE = $(\int I dt / FbMv) \times 100$, where F is Faraday's constant (965,485 C/mol e$^-$), b is the mole of electrons theoretically generated from acetate (8 mol e$^-$/mol acetate), M is the acetate concentration (mol/L), and v is the liquid volume. The current density (ID) was determined using ID = I/A, where A is the area of the anode electrode [11]. Finally, the water flux through the FO membrane was calculated using $J = \Delta V / At$, where ΔV is the catholyte (draw solution) volume change (L), A is the membrane working area (m^2), and t is the time (h).

3. Results and discussion

3.1. Morphology of FO membranes

The cross-sectional views of two FO membranes (CTA NW and PA) were observed by SEM (Fig. 2). The two FO membranes had an asymmetric structure that was composed of an active layer and a support layer. In the figure, CTA NW has a smooth active layer surface, whereas PA has a ridge-valley active layer surface, which is a typical characteristic of PA membranes formed during interfacial polymerization [12,13]. In addition, the PA active layer has a thin sponge-like structure on top of a finger-like structure. According to a previous study [12], the finger-like structure reduces the mass transfer resistance; the finger-like morphology has low tortuosity. Here, however, the active layer of CTA NW seems to be dense and less porous. The support layers of both CTA NW and PA are nonwoven fabric, and the measured thicknesses of these membranes are about 160 and 80 µm,
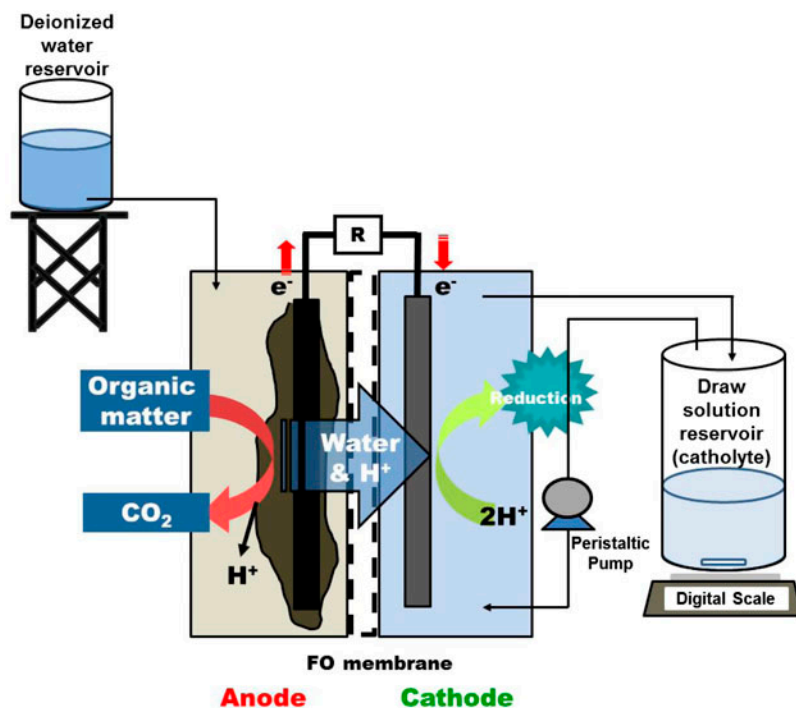
Fig. 1. Experimental setup of the FO-BES.

respectively. Based on the membrane structures and thicknesses observed by SEM, CTA NW may have a higher structural parameter (S), which is defined as $S = (t_s\tau)/\varepsilon$, where t_s is the membrane thickness, τ is the membrane tortuosity, and ε is the membrane porosity [14]. Note that S is proportionally correlated with internal concentration polarization (ICP), which reduces the FO performance [13].

3.2. Hydrophobicity of FO membranes

Contact angle measurements were conducted to determine the hydrophobicity of both the active and support layers of each FO membrane (Table 1). The active layers of CTA NW and PA displayed a similar contact angle, but the support layer of PA had a lower contact angle (84.17) than that of CTA NW (96.60). This difference indicates that the CTA NW support layer is more hydrophobic, and this greater hydrophobicity prevents the support layer from being fully wet. Consequently, effective water transport through the FO membrane can be obstructed, which would then aggravate the ICP [15]. In addition, the hydrophobic support layer can limit the access of electrolytes to the membrane surfaces [16]. We thus posit that better mass transport occurs through PA, as it has a more hydrophilic characteristic.

3.3. Electrical properties of FO membranes

To further investigate both the mass transport behavior through the FO membranes and electrical characteristics of the FO membranes, impedance spectroscopy analyses were conducted. Fig. 3 presents the impedance magnitude as a function of frequency for CTA NW and PA under static conditions (feed solution: 0.01 M NaCl; draw solution: 0.01 M NaCl) having no osmotic pressure, and dynamic conditions (feed solution: 0.01 M NaCl; draw solution: 0.5 M NaCl) having an osmotic pressure difference across the membrane. Black star symbols indicate the baseline, which are the impedance spectra for the 10 mM NaCl solution with no membrane. Under static conditions, impedance values analogous to the baseline were observed in the impedance spectrum measurements of CTA NW and PA at a high frequency range. Generally, at a high frequency range, the impedance spectra are attributed to the electrolytes and membranes [17]; thus, this result indicates that not all membranes significantly affect the impedance. On the other hand, at the low frequency range, the impedance value for CTA NW was much larger than for PA under static conditions. Impedance values at a low frequency range are caused by ion diffusion and mass transport [17]; here, CTA NW clearly has a higher mass transfer resistance than PA.
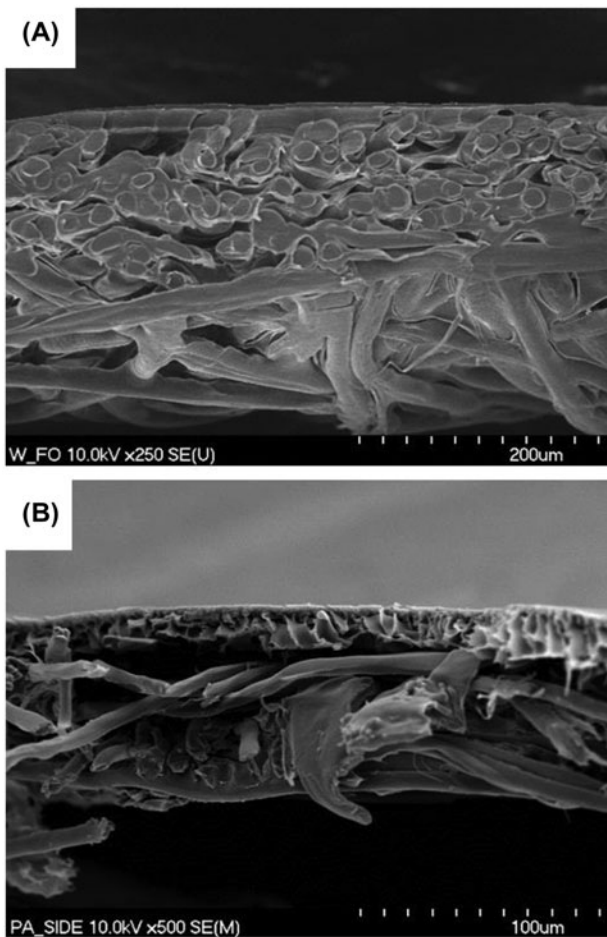
Fig. 2. Cross-sectional SEM images of (A) CTA NW and (B) PA.

Table 1
Contact angle analyses of active and support layer surfaces of CTA NW and PA

	CTA NW	PA
Active	66.10 ± 3.73	68.27 ± 4.25
Support	96.60 ± 4.75	84.17 ± 0.79

Under dynamic conditions, impedance values at the high frequency range are lower than those under static conditions, and impedance magnitudes according to membrane type and orientation were also similar to each other. It is believed that the utilization of a higher conductivity electrolyte (0.5 M NaCl) reduced the impedance magnitudes, but it was not the membrane that mainly contributed to the changes in impedance at high frequency range. In other words, the ohmic resistances of the two FO membranes are nearly identical. The dynamic condition also showed
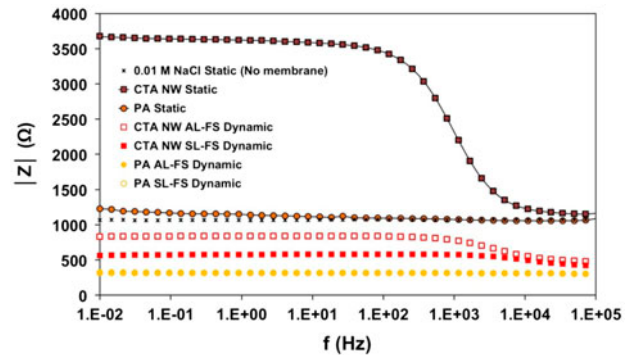

Fig. 3. Impedance magnitude of two-chamber electrodialytic cells equipped with CTA NW and PA in different membrane orientations as a function of frequency under static (with no osmotic pressure) and dynamic (with osmotic pressure) conditions.

lower impedance values at the lower frequency range; water and diffusive solute transport actively took place to maintain the mass balance across the FO membrane. Consistent with the static conditions, CTA NW showed greater impedance values than PA under dynamic conditions; the ionic species and water could not quickly transfer through CTA NW as it had a higher S value and more hydrophobic support layer.

In addition, membrane orientation seemed to affect the impedance magnitude for CTA NW at the lower frequency range. The impedance magnitude of CTA NW AL-FS was higher than for the CTA NW SL-FS, implying that improved mass transport and ion diffusion occurs through the CTA NW SL-FS. These results correspond to the higher water flux and reverse solute flux that were obtained from the test for the CTA NW SL-FS than for the CTA NW AL-FS [13]. The mass transport and ion diffusion differences ascribed to membrane orientation are likely due to the ICP pattern difference. In the CTA NW AL-FS, the dilution effect of the draw solution occurs in the porous support layer matrix [18]; the dilutive ICP reduces the accessibility of ionic species to the membrane surface and effective osmotic pressure, which is the driving force of water flux. In contrast, rather than dilutive ICP, concentrative ICP occurs in the CTA NW SL-FS, in which the draw solute increases at the boundary between the active and support layers [19]. The ICP in the CTA NW SL-FS is generally smaller than for the CTA NW AL-FS; therefore, a higher flux and ion diffusion were obtained in the CTA NW SL-FS [19]. However, in terms of PA, membrane orientation did not significantly affect the impedance magnitude at the lower frequency range; the lower membrane thickness and the increase in the hydrophilic support layer of PA might reduce the ICP phenomena.

3.4. Proton transport through FO membranes

One of the main reasons electricity generation deteriorates in BESs is the pH gradient between the anode and cathode chambers because of the poor proton transport ability of the cation exchange membrane, which is a representative separator in BESs [9]. The proton transport through CTA NW and PA in different membrane orientations was evaluated in a two-chamber abiotic cell (feed solution: 0.05 M PBS at pH 7; draw solution: 0.6 M NaCl at pH 7). Fig. 4 shows the pH changes in the draw solution. Regardless of the membrane orientation, the most active proton transport occurred through PA. However, in terms of CTA NW, the SL-FS orientation displayed a better proton transport ability than the AL-FS orientation, which is consistent with the results of impedance measurements under dynamic conditions.

3.5. Electricity production in FO-BESs

The current generated was measured during FO-BES operation with CTA NW and PA in different orientations, including AL-FS and SL-FS (Fig. 5). During the first batch cycle, similar maximum ID were observed in the FO-BES with PA in SL-FS (561.2 mA/m^2) and with CTA NW in SL-FS (559.2 mA/m^2). The FO-BES with PA in AL-FS displayed a slightly lower maximum ID (503.0 mA/m^2), whereas the FO-BES with CTA NW in AL-FS recorded a much lower maximum ID (374.7 mA/m^2). The reason why the FO-BES with CTA NW in AL-FS showed the lowest maximum ID during the first batch cycle is likely due to severe dilutive ICP. The CTA NW membrane has a thick nonwoven porous support layer, leading to a degradation of electrolyte species mobility [17].
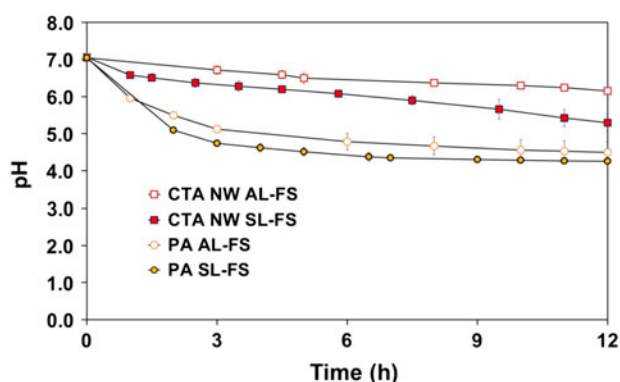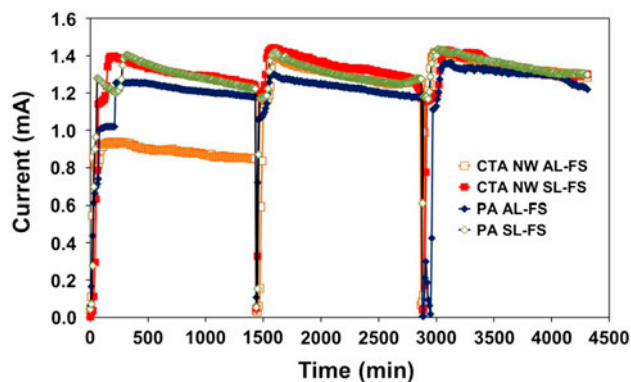
Fig. 5. Current output in the FO-BESs having two different FO membranes during the three batch cycles.

Unlike the first batch cycle, during the second and third batch cycles, regardless of membrane types and orientations, similar maximum IDs (CTA NW AL-FS: 558.1 and 566.5 mA/m^2; CTA NW SL-FS: 559.2 and 571.1 mA/m^2; PA AL-FS: 520.0 and 545.5 mA/ m^2; PA SL-FS: 567.9 and 573.5 mA/m^2) were observed in the FO-BESs, although PA displayed a better proton transport ability and smaller mass transport resistance in the membrane characterization experiments.

In addition, the maximum ID increased as the FO-BES batch cycles were increased. For example, the ID of FO-BES with PA AL-FS in the second batch cycle increased slightly relative to the first batch cycle. These increases in maximum ID are opposite to the water flux (Fig. 7), which decreased with further batch cycles, possibly due to membrane fouling as it increases ion transport through the FO membrane. In a previous study, a FO-BES with a fouled FO membrane showed a higher current density than for a virgin FO membrane, although a FO-BES having a fouled FO membrane had no water flux [6]. However, few studies on the relationship between membrane fouling and salt flux have been explored; further studies are required to clarify this phenomenon.

As shown in Fig. 6, in terms of the CE, except for the first batch operation of the FO-BES CTA NW AL-FS (24.3%), approximately a 35.4% CE was observed during all the batch operations. The CE of the FO-BES was comparatively lower than reported in previous studies, which used the same reactor design (65%) [20]. This finding may be attributed to the unfavorable transfer of acetate from the anode to cathode chambers through all FO membranes observed during the FO-BES operation. Preventing the leakage of acetate through FO membranes would be one of the main challenges for future FO-BES.

Fig. 4. pH changes in NaCl solution used as draw solution in two-chamber abiotic cell for proton transport test.
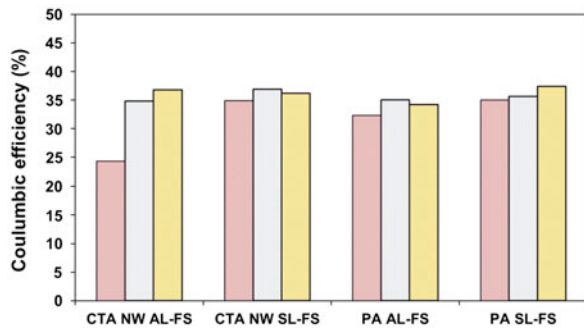
Fig. 6. CE of FO-BESs having two FO membranes in different membrane orientations.
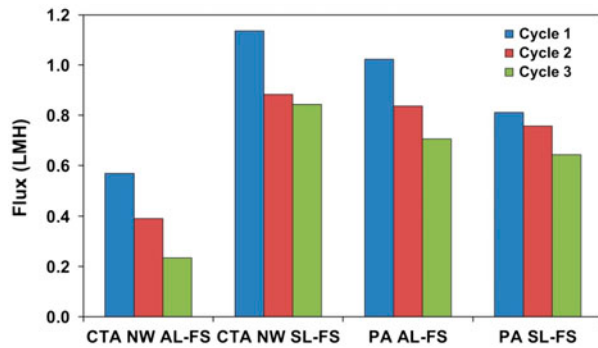

Fig. 7. Water flux through FO membranes in different orientations during FO-BES operation.

3.6. Water flux through membranes in FO-BES

Water flux was measured during FO-BES operation (Fig. 7). The FO-BES having a CTA NW AL-FS had the lowest water flux (0.57–0.23 LMH), followed by PA SL-FS (0.81–0.64 LMH), PA AL-FS (1.02–0.70 LMH), and CTA NW SL-FS (1.13–0.84 LMH). The reason for the lowest water flux in the FO-BES having CTA NW AL-FS can be explained by the severe dilutive ICP. The intriguing aspect of this result is that a higher water flux was observed in the FO-BES with CTA SL-FS than with PA, even though PA was expected to have a lower S value in the membrane characterization experiments. The inner environment of the FO-BES is more complicated than typical FO processes due to additional installations, such as electrodes; as such, the water flux might be affected by other factors.

4. Conclusions

In this study, CTA NW and PA FO membranes were characterized, and the performances of FO-BESs having these two membranes were compared. CTA NW had a larger thickness than PA, and the support

layer of CTA NW was more hydrophobic than that of PA. These properties of CTA NW led to a larger S value, which reduced ion diffusion and mass transport. The electric properties determined by impedance spectrum measurements were consistent with information derived from the physical properties of the membranes. It was also found that dynamic conditions (i.e. the presence of osmotic pressure) reduced the mass transport resistance across the FO membranes. The results of the electrical property determination confirmed that there were no considerable differences between the CTA and PA membrane ohmic resistances, though the CTA NW AL-FS had the largest mass transfer resistance. Increased active proton transport was observed in the PA AL-FS and SL-FS. Based on the membrane characteristics, the FO-BESs with the PA AL-FS and SL-FS seemed to achieve better current generation and a higher water flux. However, during actual operation of the FO-BES, current generation was not significantly affected by membrane type or orientation. Moreover, the FO-BES having the CTA NW SL-FS showed the highest flux; based on the overall findings, CTA NW in AL-FS orientation is recommended for the better performance of the FO-BES. The reason for the difference in the result between the characterization test and actual FO-BES operation may be attributed to the more complex internal environment of the FO-BES due to the presence of microorganisms and electrodes, aeration to the cathode, and gas generation (methane and carbon dioxide) in the anode. Therefore, for a further understanding of internal phenomena in FO-BESs having different FO membranes in different orientations, an investigation into these variations is required.

References

[1] M. Hejazi, J. Edmonds, L. Clarke, P. Kyle, E. Davies, V. Chaturvedi, M. Wise, P. Patel, J. Eom, K. Calvin, R. Moss, S. Kim, Long-term global water projections using six socioeconomic scenarios in an integrated assessment modeling framework, Technol. Forecast. Soc. 81 (2014) 205–226.

[2] M. Elimelech, W.A. Phillip, The future of seawater desalination: Energy, technology, and the environment, Science 333 (2011) 712–717.

[3] Q. Schiermeier, Water: Purification with a pinch of salt, Nature 452 (2008) 260–261.

[4] T.-S. Chung, X. Li, R.C. Ong, Q. Ge, H. Wang, G. Han, Emerging forward osmosis (FO) technologies and challenges ahead for clean water and clean energy applications, Curr. Opin. Chem. Eng. 1 (2012) 246–257.

[5] C.M. Werner, B.E. Logan, P.E. Saikaly, G.L. Amy, Wastewater treatment, energy recovery and desalination using a forward osmosis membrane in an air-cathode microbial osmotic fuel cell, J. Membr. Sci. 428 (2013) 116–122.

[6] Z. Ge, Z. He, Effects of draw solutions and membrane conditions on electricity generation and water flux in osmotic microbial fuel cells, Bioresour. Technol. 109 (2012) 70–76.

[7] Z. Ge, Q. Ping, L. Xiao, Z. He, Reducing effluent discharge and recovering bioenergy in an osmotic microbial fuel cell treating domestic wastewater, Desalination 312 (2013) 52–59.

[8] F. Zhang, K.S. Brastad, Z. He, Integrating forward osmosis into microbial fuel cells for wastewater treatment, water extraction and bioelectricity generation, Environ. Sci. Technol. 45 (2011) 6690–6696.

[9] K.J. Chae, M. Choi, F.F. Ajayi, W. Park, I.S. Chang, I.S. Kim, Mass transport through a proton exchange membrane (Nafion) in microbial fuel cells, Energy Fuels 22 (2008) 169–176.

[10] M.-J. Choi, K.-J. Chae, F.F. Ajayi, K.-Y. Kim, H.-W. Yu, C.-W. Kim, I.S. Kim, Effects of biofouling on ion transport through cation exchange membranes and microbial fuel cell performance, Bioresour. Technol. 102 (2011) 298–303.

[11] S. Oh, B. Min, B.E. Logan, Cathode performance as a factor in electricity generation in microbial fuel cells, Environ. Sci. Technol. 38 (2004) 4900–4904.

[12] N.Y. Yip, A. Tiraferri, W.A. Phillip, J.D. Schiffman, M. Elimelech, High performance thin-film composite forward osmosis membrane, Environ. Sci. Technol. 44 (2010) 3812–3818.

[13] J. Wei, C. Qiu, C.Y. Tang, R. Wang, A.G. Fane, Synthesis and characterization of flat-sheet thin film composite forward osmosis membranes, J. Membr. Sci. 372 (2011) 292–302.

[14] J.R. McCutcheon, M. Elimelech, Influence of concentrative and dilutive internal concentration polarization on flux behavior in forward osmosis, J. Membr. Sci. 284 (2006) 237–247.

[15] J.R. McCutcheon, M. Elimelech, Influence of membrane support layer hydrophobicity on water flux in osmotically driven membrane processes, J. Membr. Sci. 318 (2008) 458–466.

[16] K.-Y. Kim, E. Yang, M.-Y. Lee, K.-J. Chae, C.-M. Kim, I.S. Kim, Polydopamine coating effects on ultrafiltration membrane to enhance power density and mitigate biofouling of ultrafiltration microbial fuel cells (UF-MFCs), Water Res. 54 (2014) 62–68.

[17] Y. Gao, W. Li, W.C. Lay, H.G. Coster, A.G. Fane, C.Y. Tang, Characterization of forward osmosis membranes by electrochemical impedance spectroscopy, Desalination 312 (2013) 45–51.

[18] I.L. Alsvik, M.-B. Hägg, Pressure retarded osmosis and forward osmosis membranes: Materials and methods, Polymers 5 (2013) 303–327.

[19] G.T. Gray, J.R. McCutcheon, M. Elimelech, Internal concentration polarization in forward osmosis: Role of membrane orientation, Desalination 197 (2006) 1–8.

[20] K.J. Chae, M.J. Choi, J.W. Lee, K.Y. Kim, I.S. Kim, Effect of different substrates on the performance, bacterial diversity, and bacterial viability in microbial fuel cells, Bioresour. Technol. 100 (2009) 3518–3525.